Flight Dynamics Aspects of a Large Civil Tiltrotor Simulation using Translational Rate Command

Ben Lawrence
San Jose State University Research
Foundation
Ames Research Center
Moffett Field, CA
Ben.lawrence@nasa.gov

Carlos A. Malpica
Colin R. Theodore
William A. Decker
NASA
Ames Research Center
Moffett Field, CA
Carlos.a.malpica@nasa.gov
Colin.theodore@nasa.gov

James E. Lindsey
Monterey Technologies
Monterey, CA
Ames Research Center
James.e.lindsey@nasa.gov

ABSTRACT

An in-depth analysis of a Large Civil Tiltrotor simulation with a Translational Rate Command control law that uses automatic nacelle deflections for longitudinal velocity control and lateral cyclic for lateral velocity control is presented. Results from piloted real-time simulation experiments and offline time and frequency domain analyses are used to investigate the fundamental flight dynamic and control mechanisms of the control law. The baseline Translational Rate Command conferred handling qualities improvements over an attitude command attitude hold control law but in some scenarios there was a tendency to enter PIO. Nacelle actuator rate limiting strongly influenced the PIO tendency and reducing the rate limits degraded the handling qualities further. Counterintuitively, increasing rate limits also led to a worsening of the handling qualities ratings. This led to the identification of a nacelle rate to rotor longitudinal flapping coupling effect that induced undesired pitching motions proportional to the allowable amount of nacelle rate. A modification that applied a counteracting amount of longitudinal cyclic proportional to the nacelle rate significantly improved the handling qualities. The lateral axis of the Translational Rate Command conferred Level 1 handling qualities in a Lateral Reposition maneuver. Analysis of the influence of the modeling fidelity on the lateral flapping angles is presented. It is showed that the linear modeling approximation is likely to have under-predicted the side-force and therefore under-predicted the lateral flapping at velocities above 15 ft/s. However, at lower velocities, and therefore more weakly influenced by the side force modeling, the accelerations that the control law commands also significantly influenced the peak levels of lateral flapping achieved.

NOTATION

a_y	Aircraft body Y-axis acceleration
g	Acceleration due to Gravity
K	Nacelle rate to longitudinal cyclic crossfeed gain
m	Aircraft Mass
$M_{\beta_{1c}}$	Stability Derivative, pitching acceleration due to rotor longitudinal flapping
$p\ q\ r$	Body axes angular rates
T	Rotor thrust
$u\ v\ w$	Body axes X, Y and Z velocities
$X_{\beta_{1c}}$	Stability Derivative, longitudinal acceleration due to rotor longitudinal flapping
X_{β_m}	Stability Derivative, longitudinal acceleration due to nacelle angle

X_u	Stability Derivative, longitudinal acceleration due to longitudinal velocity
Y_v	Stability Derivative, lateral acceleration due to lateral velocity
$\beta_{1c_{1,2}}$	Rotor longitudinal flapping angle (rotor 1,2)
$\beta_{1s_{1,2}}$	Rotor lateral flapping angle (rotor 1,2)
β_m	Nacelle angular displacement
$\dot\beta_m$	Nacelle angular rate
$\dot\beta_{1c_{\dot\beta_m}}$	Stability Derivative, rotor longitudinal flapping acceleration due to nacelle rate
$\dot\beta_{1c_{\theta_{1s}}}$	Stability Derivative, rotor longitudinal flapping acceleration due to longitudinal cyclic angle
$\dot\beta_{1c_q}$	Stability Derivative, rotor longitudinal flapping acceleration due to pitch rate
θ, φ	Pitch, Roll Euler angles
θ_{1s}	Longitudinal cyclic angle

INTRODUCTION

NASA's Subsonic Rotary Wing Program is researching technologies to radically improve the capabilities and civil benefits of rotary-wing vehicles. This has led to research into large size, heavy lift tiltrotors for a future V/STOL civil transport vehicle. This is seen as the most promising advanced rotorcraft configuration [1] to meet future airspace requirements for capacity, flexibility, emissions, efficiency and safety, such as those laid out in the FAA's NEXTGEN vision (www.faa.gov/nextgen). The Large Civil Tiltrotor 2 (LCTR2) is a concept design that acts as a focal point for a range of rotorcraft research disciplines. The LCTR2 is a large rotorcraft, weighing about 100,000lbs with a 107ft wingspan and two tilting nacelles with 65ft diameter rotors [2]. This aircraft, being significantly heavier and larger than any existing tiltrotor, poses a number of fundamental questions with respect to handling qualities characteristics and flight control requirements. Recent handling qualities research [3], [4] has worked on addressing these fundamental questions for the hover and low-speed regime and the work presented herein is a continuation of this campaign.
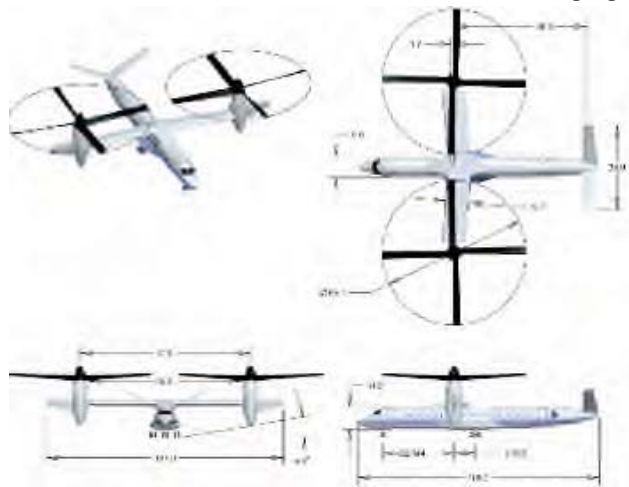

Figure 1: NASA Large Civil Tiltrotor (LCTR2)

This paper presents an analysis of certain flight dynamics and control aspects of a real-time capable simulation of the LCTR2, [5], in hover and low speed maneuvering. The analysis focuses on the application of a Translational Rate Command (TRC) control law that uses automatic nacelle angle and parallel lateral cyclic inputs to control longitudinal and lateral velocity respectively and seeks to investigate the driving factors behind the results of piloted handling qualities simulations that assessed the TRC control laws in the NASA Vertical Motion Simulator (VMS). The reader is directed to ref [6] for a complete description of the experimental setup, test matrix and experimental conduct.

The piloted simulations were aimed at investigating whether TRC could improve the hover and low speed handling qualities over what was achieved with Attitude Command Attitude Hold (ACAH) control laws used previously [3], [4]. The main premise for TRC was that it enabled control of the aircraft with minimal attitude changes. This provided a potential solution to a deficiency encountered in earlier experiments where using ACAH induced large and unsatisfactory accelerations at the pilotstation (with aircraft pitch or yaw) which was positioned a long way (~40ft) from the center of rotation. The goal was to investigate the 'art of the possible' i.e. did this type of TRC control law confer the desired handling qualities improvements? And if it did, what levels of nacelle angle actuation rates/angles would be necessary to provide these handling qualities?

The paper comprises two main parts; the first considers the longitudinal dynamics and control of the aircraft under TRC control in a modified version of the ADS-33E Precision Hover Mission Task Element (MTE) [7]. The modifications to make the MTE more 'appropriate' for this type of aircraft and its role are documented in detail in ref [4]. However the key changes to the Cargo/Utility performance standards with a 1ft increase in the *desired* longitudinal, lateral and height position standards (±4ft, ±4ft, ±3ft), and double these for *adequate* performance. All the maneuvers were flown at 52 ft radar altitude, an increase over the standard ADS-33E value. Although the Hover MTE is a multi-axis task, the predominant handling qualities issues were the tracking and capture of the longitudinal velocity and position. The paper considers various aspects of using nacelle motion to control longitudinal translational motion including varying the nacelle rate and position actuation limits and the effects of longitudinal rotor flapping induced by the nacelle motion.

The second part considers the lateral axis of the TRC control law in the ADS-33E Lateral Reposition MTE [7], where the specific focus is the lateral flapping behavior during the maneuver. The simplified linear model used, which although representative at hover, may have under-predicted the side-force (and thus rotor flapping) as the lateral velocity increased. The analysis investigates the sensitivity of the results to this modeling aspect and presents comparisons of the aircraft and rotor flapping response for the three control laws: ACAH, TRC, and a 'Hybrid' mode that combines ACAH and TRC.

The paper will conclude with lessons learnt from the use of this form of TRC control and assessments of the important factors its implementation for handling qualities aspects.

Modeling aspects will also be addressed, highlighting the important assumptions and an assessment of their impact.

LCTR SIMULATION MODEL

The LCTR2 simulation model used a qLPV (quasi-Linear Parameter Varying) or 'stitched' [8] modeling approach that combined multiple 13-state linear stability derivative-based state-space models to provide varying model dynamics and trim characteristics for changing flight speed and nacelle angle [5]. The model states consisted of nine body states $[u, v, w, p, q, r, \varphi, \theta, \psi]$ representing the 2nd order rigid-body dynamics, and four rotor states, $[\beta_{1s_1}, \beta_{1s_2}, \beta_{1c_1}, \beta_{1c_2}]$ providing a first-order representation of flapping dynamics. The envelope of the model was valid for hover and low speed (0-60kts) and for nacelle angles between 60 and 95 degrees. The bare airframe qLPV model was integrated into a model following control system architecture as shown in Figure 2. Note also the inclusion of the CETI turbulence model, [9] which was used for all evaluation runs, with parameters set for a moderate level of turbulence [6].
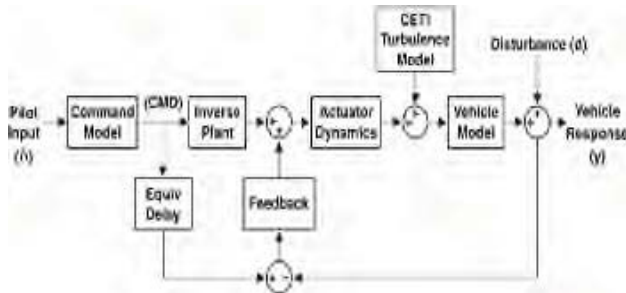

Figure 2: Model-following control architecture

The control system architecture was used for both ACAH and TRC control modes. The architecture consists of two key functions: 1. A feedback or regulator path which tries to minimize the error between the desired and measured aircraft response and 2: A command and inverse plant model which convert stick inputs to idealized responses and then to swashplate inputs. The swashplate actuator models featured rate limiting whilst the nacelle actuators were modeled as second order systems with both angular position and rate limiting. The nacelle actuator natural frequency was selected at high enough value (8 rad/s) to minimize interference with the primary aircraft modes.

The TRC mode actuates the nacelles to control longitudinal velocity and the model is designed to allow experimental variation of the nacelle actuator rate and angular position limits. The lateral velocity is controlled using parallel lateral cyclic on both rotors. The maximum stick deflection was ±5 inches and the control law has a baseline stick sensitivity of 15ft/s/inch for both the longitudinal and lateral velocity. This sensitivity is based on the fact that the TRC is primarily aimed at improving precision hover HQ's and pilot feedback in the development phase favored maximum typical stick displacements in the maneuver of just over an inch leading to a 'useful' velocity range of around ±18ft/s (11kts) .

For lateral TRC, an addition to the 'pure' mode where translation is commanded whilst the roll attitude is held close to zero was a combined TRC/ACAH control mode where the pilot input commands lateral velocity and roll attitude changes simultaneously. This allowed the investigation of pilot preference of the aircraft response type as well as the tradeoff between rotor flapping and attitude response.

Initially, a small 'thumb stick' on the pilot's Thrust Control Lever (TCL) was configured to be the primary TRC inceptor for the piloted experiments. However, an option of commanding the TRC via the center stick was also implemented which, after initial experimentation, became the preferred method and all the results discussed in this paper use this inceptor.

LONGITUDINAL TRC IN THE HOVER

The initial results showed that the TRC generally improved the handling qualities but that a handling qualities 'cliff' existed where, under certain circumstances, piloted induced oscillations (PIO's) in longitudinal control were encountered. Figure 3 shows a comparison of two runs from the piloted experiments flying the Hover MTE, one showing a successful capture of the hover point and another resulting in a PIO. These runs are from different pilots both using the baseline TRC control system with ±7.5 deg/sec nacelle rate limit and angular position limits at 95 deg aft and 77 deg forwards (90 deg being the vertical position). Initially, both maneuvers are flown very similarly, with equivalent amounts of stick input used and approach speeds attained.
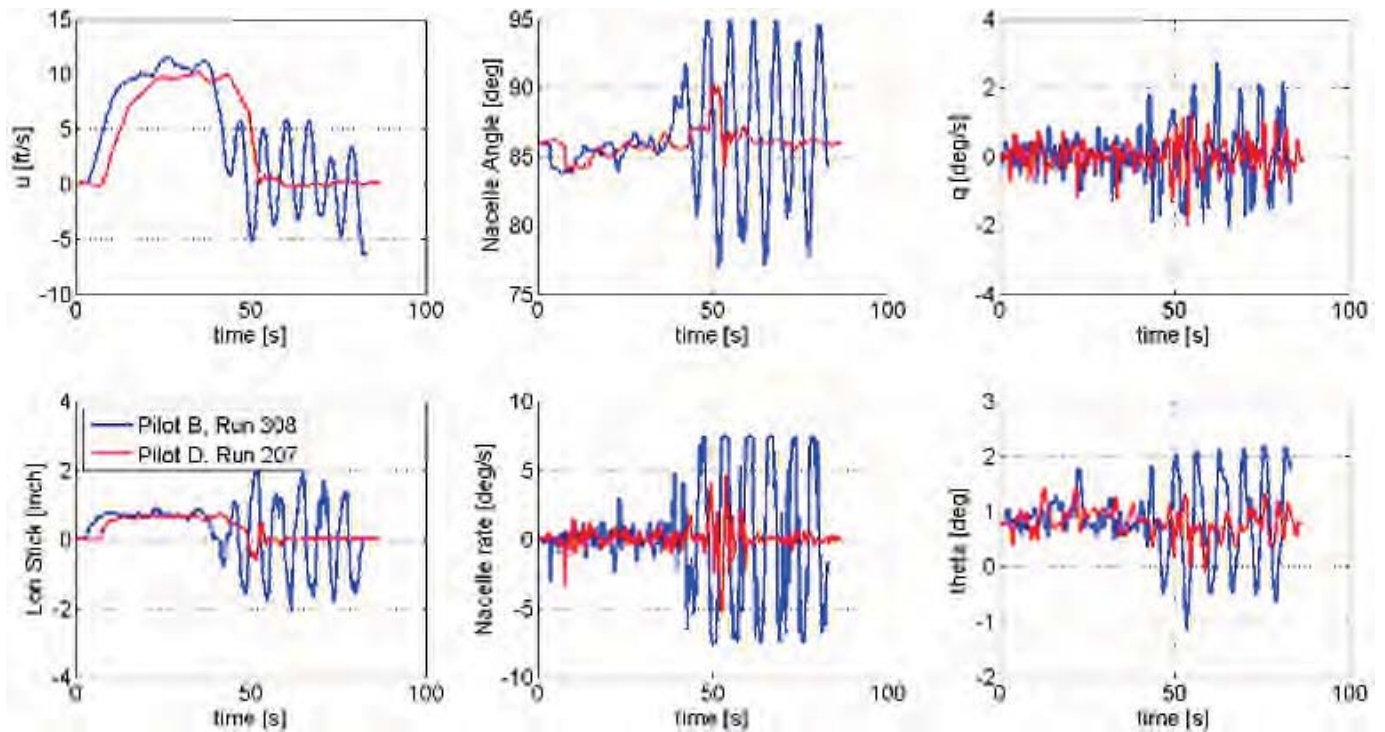
Figure 3: VMS piloted simulation experiments in the Precision Hover MTE using TRC, one showing a successful capture of hover point (pilot D) and another resulting in a PIO (Pilot B)

The differences occur at the point where the aircraft decelerate back to hover. For Pilot D, after the initial large stick reversal input to slow down, the pilot is able to smoothly bring the aircraft to hover with a further 1 to 2 discrete correcting inputs. However, Pilot B makes a slightly larger and more 'aggressive' (greater rate of change) input to decelerate which causes a correspondingly larger nacelle angle change, peaking at around 92 degrees (6 degrees aft of the 86 degree trim datum at hover). The consequent deceleration is more rapid and demands a greater nacelle actuation rate. This is followed by even larger stick input in the opposite direction – this appears to be the trigger point for the PIO, after which a classical 'saw-tooth' time history of the nacelle actuator angle is observed with the actuator reaching both the position and rate limits. The PIO in this case was very prolonged, with the pilot staying 'in-the-loop' for 20-25secs. This is typical of the results from the experiments where relatively subtle changes in events could lead to quite different outcomes, with a large or over-aggressive input the most likely trigger for the PIOs.

Handling Qualities Results

The average HQRs awarded for the 'baseline' TRC control law configurations in the Hover MTE are presented in Figure 4 and are compared to those awarded for the ACAH control law. The general trend is a slight improvement when moving from ACAH to TRC.

However, the spread of the HQRs, denoted by the error bars, indicates a large variability for the ratings for each control law and the presence of the HQ cliff. Figure 4 also introduces a further implementation of the TRC control law that includes a crossfeed between nacelle angular rate to longitudinal cyclic. This implementation of TRC is termed 'improved' TRC and is discussed later in this paper.
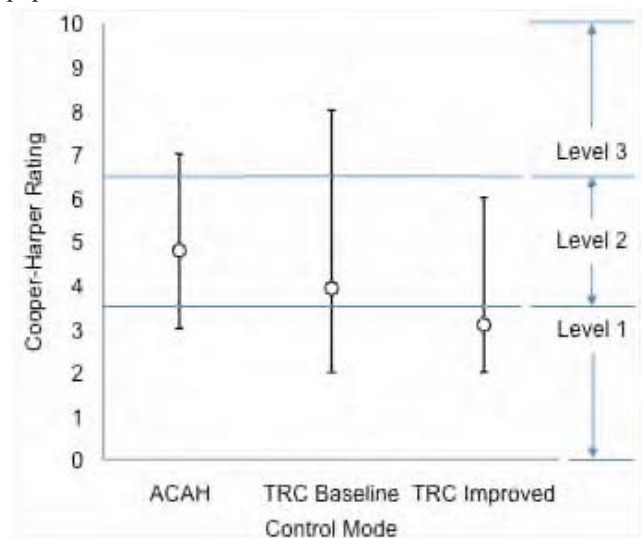

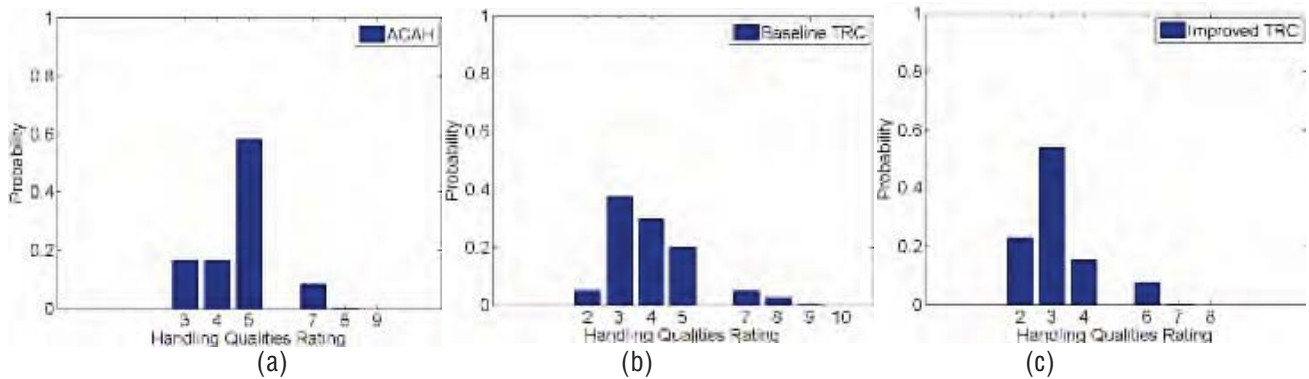Figure 4: Handling Qualities Ratings for ACAH, 'baseline' TRC, and 'improved' TRC control laws

Figure 5: **Likelihood analysis showing probability of awarded HQR for ACAH, 'baseline' TRC, and 'improved'** TRC control laws

An alternative way of presenting the HQR results uses a likelihood function as developed by Bradley and MacClaren in Ref [10]. The technique uses an ordinal logistic regression method and allows the specifying and fitting of regression relationships between ordered categorical response variables and explanatory variables. In this case, the response variable is the HQR on an ordered categorical scale of 1 to 10 which corresponds to the Cooper-Harper Handling Qualities Ratings [11]. The explanatory variables are the experimental factors, such as the control law configuration, MTE, etc, i.e. any parameter believed to influence the rating. The method uses an input dataset to compute probabilities for the likelihood that a particular HQR will be awarded for particular combination of experimental factors.

Figure 5, (a), (b) and (c) compare the computed HQR likelihood in the Precision Hover MTE for three control system configurations: ACAH, the baseline TRC, and the improved TRC control laws. The technique provides useful additional insight including giving a sense of the distribution of the variability in the results.

For example, Figure 5(a) shows that, based on the dataset available (Hover MTE, all 10 pilots), there is approximately a 60% likelihood of the ACAH configuration being a HQR 5, with smaller probabilities for HQR 3 & 4 (~15%) and for HQR 7 (<10%). For the baseline TRC model, in Figure 2(b), the probabilities are more spread out. However, the likelihood of the HQR being awarded 4 or better is approximately 75% (HQR4:

30% + HQR3: 40% + HQR2: 5%) – supporting the initial assessment of TRC generally conferring a HQ improvement over ACAH. The remaining 25% indicates that there is a smaller but not insignificant chance of this configuration being awarded a HQR 5 or worse. The spread of the rating probabilities indicate that around 50% of the time Level 1 HQ's can be achieved, but in some circumstances they degrade. Finally, Figure 5(c) shows that the variability in the HQRs is reduced for the improved TRC control, and a more definite improvement of the HQRs to ACAH is observed. Now there is a 75-80% probability for a Level 1 rating (HQR1-3) including a 25% probability of a HQR2. There is a 20-25% probability of a HQR4 or worse being awarded – signifying that, even with this improved version, there might still be some pilots that encounter HQ issues.

The flight control and dynamics issues that drive the handling qualities ratings of the various TRC control law versions were examined, including the influence of varying the nacelle actuation rate and position limits. The results in Figure 6 show the breakdown of the HQR probabilities for changes in nacelle limits for both the baseline and improved TRC. They reflect similar trends to those in Figure 5 which only considered the nacelle rate of ±7.5 deg/s. The baseline model exhibits a spread of HQR probabilities whereas the improved TRC is much more tightly clustered in and around the Level 1 region (HQR 1-3). The reasons for this improvement will be discussed later in this section.
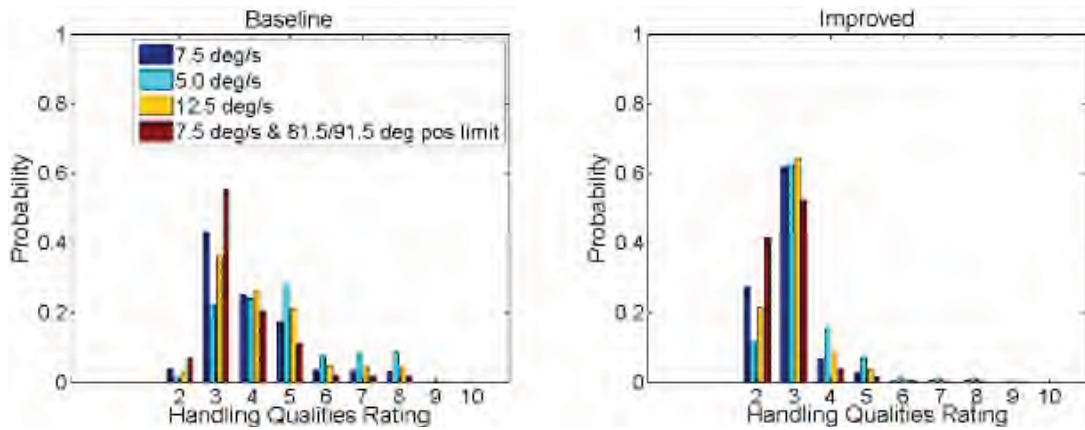
Figure 6: Likelihood analysis showing probability of HQR for various sub-configurations of the baseline and improved TRC control laws
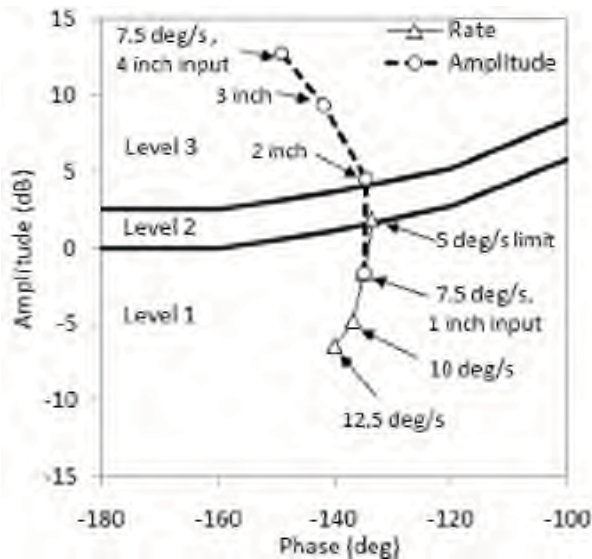

Figure 7: OLOP specifications for varying nacelle rate limits and pilot input amplitude

## Nacelle Actuation Limit Effects

Reducing the nacelle rate limits was expected to degrade the handling qualities by reducing the bandwidth available. The relationship between rate-limiting, PIOs, and the subsequent degradation of handling qualities is well established [12] [13]. Dynamic response criteria such as the Open-Loop Onset Point (OLOP) [14] are a useful predictor of the likelihood of handling qualities deficiencies due to system rate limits.

Figure 7 shows the effect of the nacelle rate limits and maximum control input on the OLOP phase and amplitude criteria and show that although the baseline 7.5 deg/s rate was Level 1 for a 1 inch magnitude stick input, an increase in stick amplitude to 2 inches and above pushes it into Level 3. Figure 8 (a) shows the frequency response of the baseline TRC control law for varying input

amplitudes. The sweeps were performed offline with the same model used in the piloted experiments using sinusoidal chirp inputs. The figures also indicate the gain and phase bandwidths for each frequency response. As the input amplitude was increased, a point is reached where there is marked drop in the phase bandwidth. At higher frequencies of around 2.5 rad/s and above, all the responses converge to the same phase curve. Here, all the system phase dynamics are dominated by the nacelle actuator natural frequency, and follow a classic second order system phase roll-off. However, at frequencies around 2 rad/s and lower, there are more significance differences, where the observed phase 'droop' becomes more pronounced with increasing input amplitude.

The gain responses show increased attenuation of the response with increasing input amplitude. This can be seen in the time response in Figure 8 (b) where at low frequencies, the velocity responses are distinct from each other and proportional to the input amplitude, but as the input frequency increases the velocity responses become almost equal irrespective of the input amplitude. Thus the magnitude curves reflect the differing input/output magnitude ratios. The exception to this is the 0.1 inch input case which never reaches the nacelle position or rate limits.

As the inputs are increased from 1 inch and greater, the effects of the nacelle actuation limits occur at different frequencies. Position limiting occurs for the 2 and 3 inch inputs at lower frequencies of about 0.35-1.2 rad/s (20-60s in the time response) – at higher frequencies the limits are no longer reached. Rate limiting initiates for the 1, 2 and 3 inch inputs at frequencies of approximately 1.2, 0.6, and 0.35 rad/s respectively and continues as the frequency is increased.
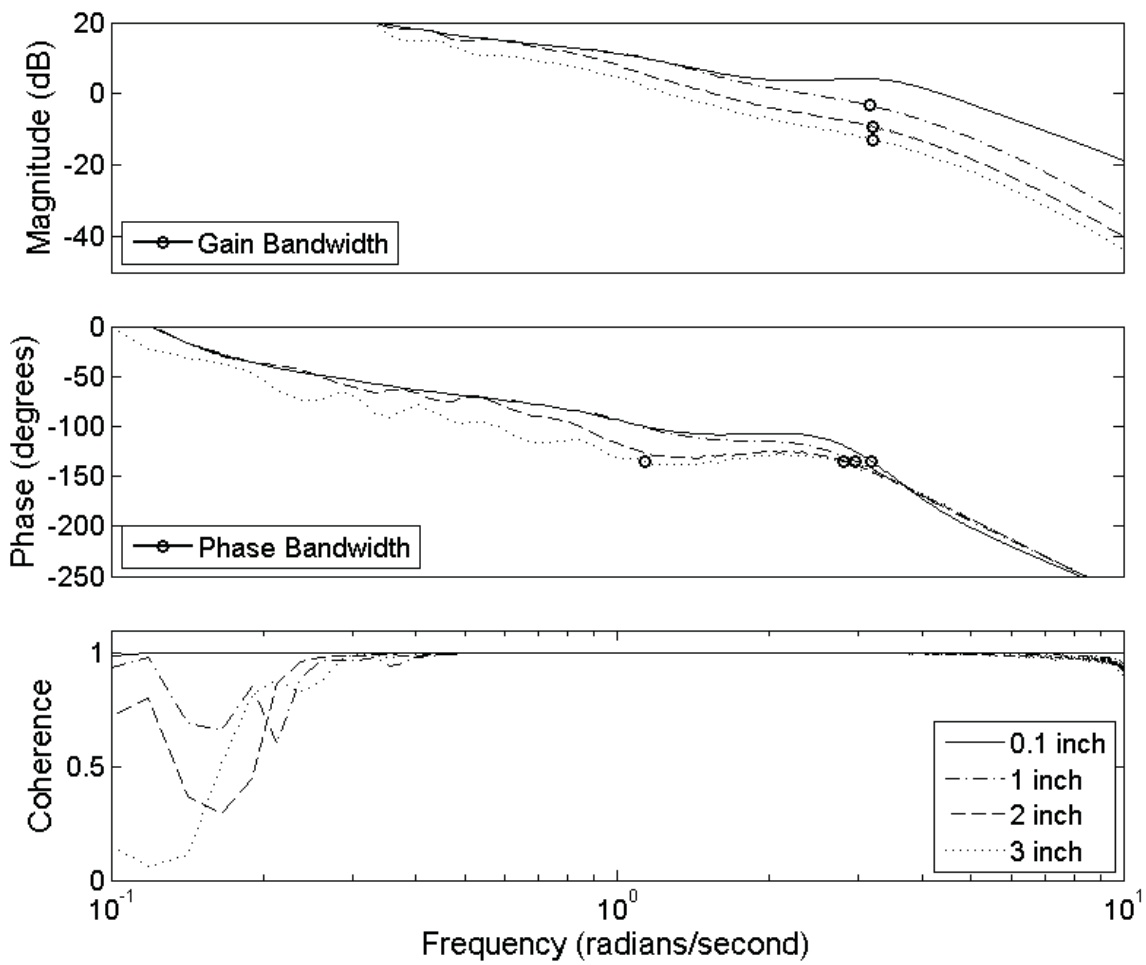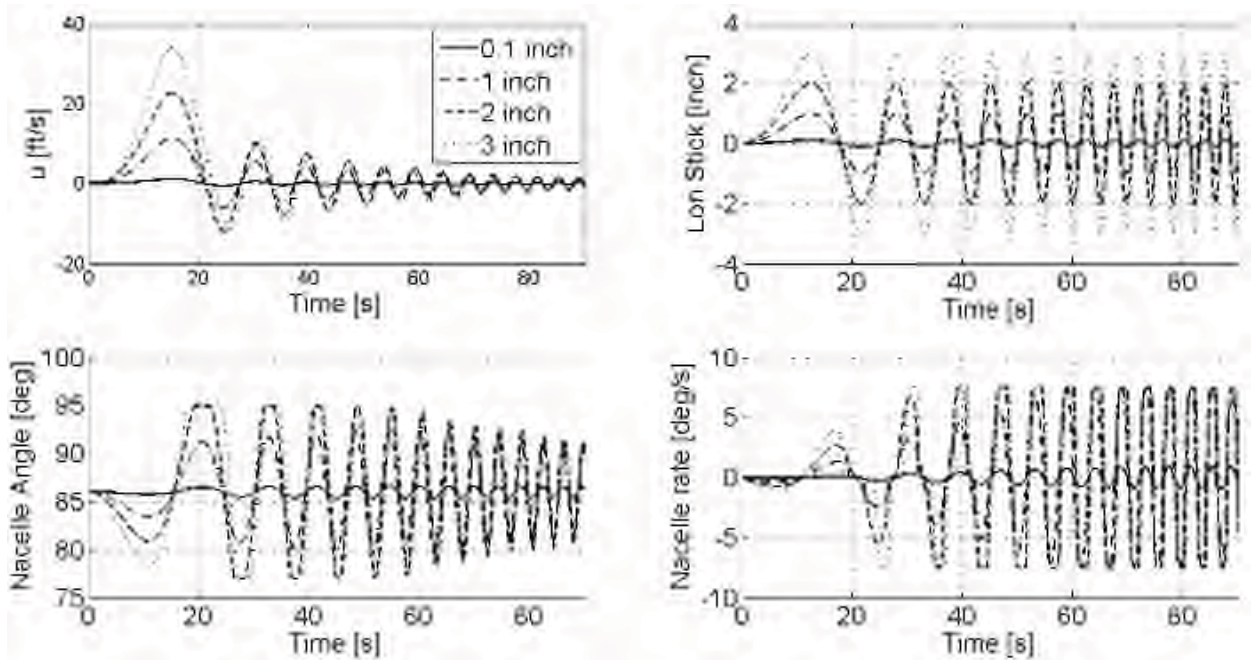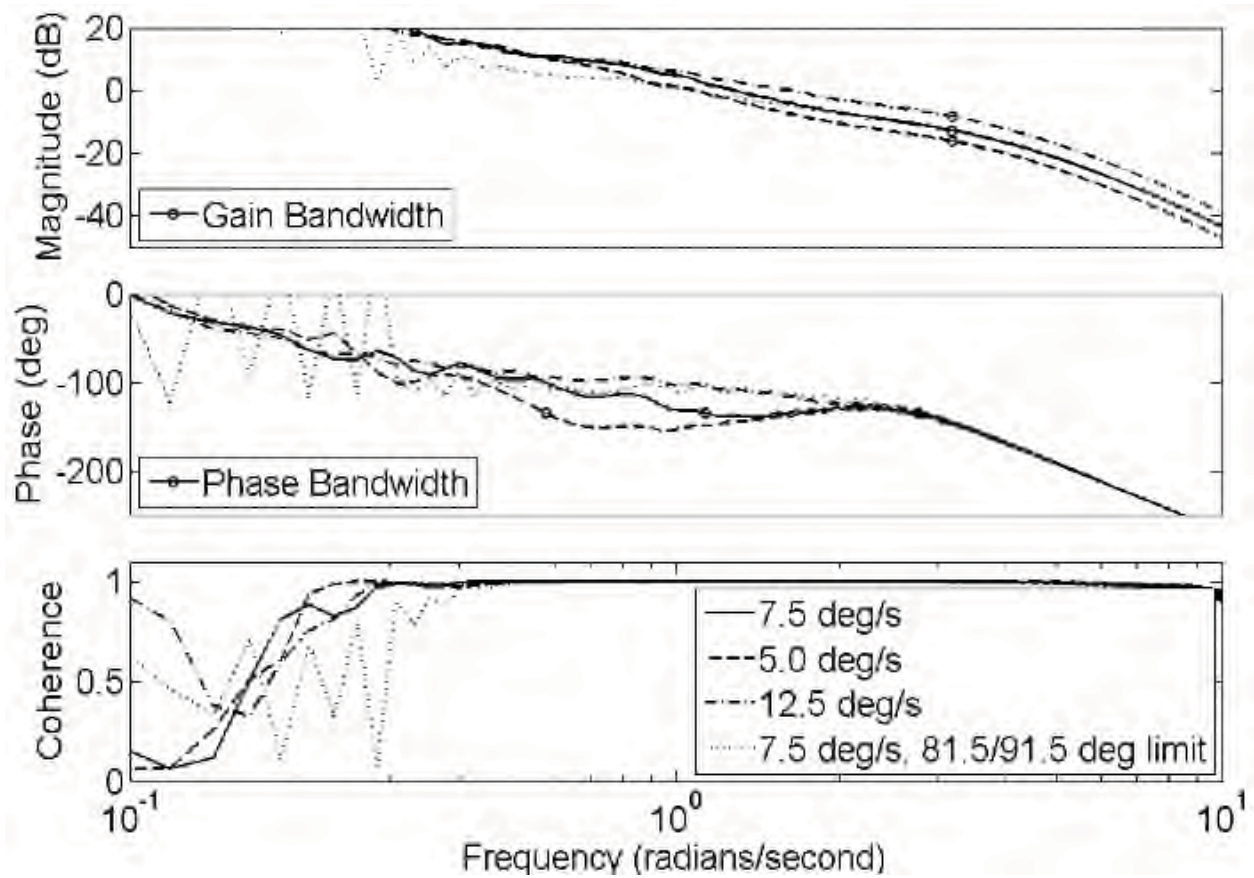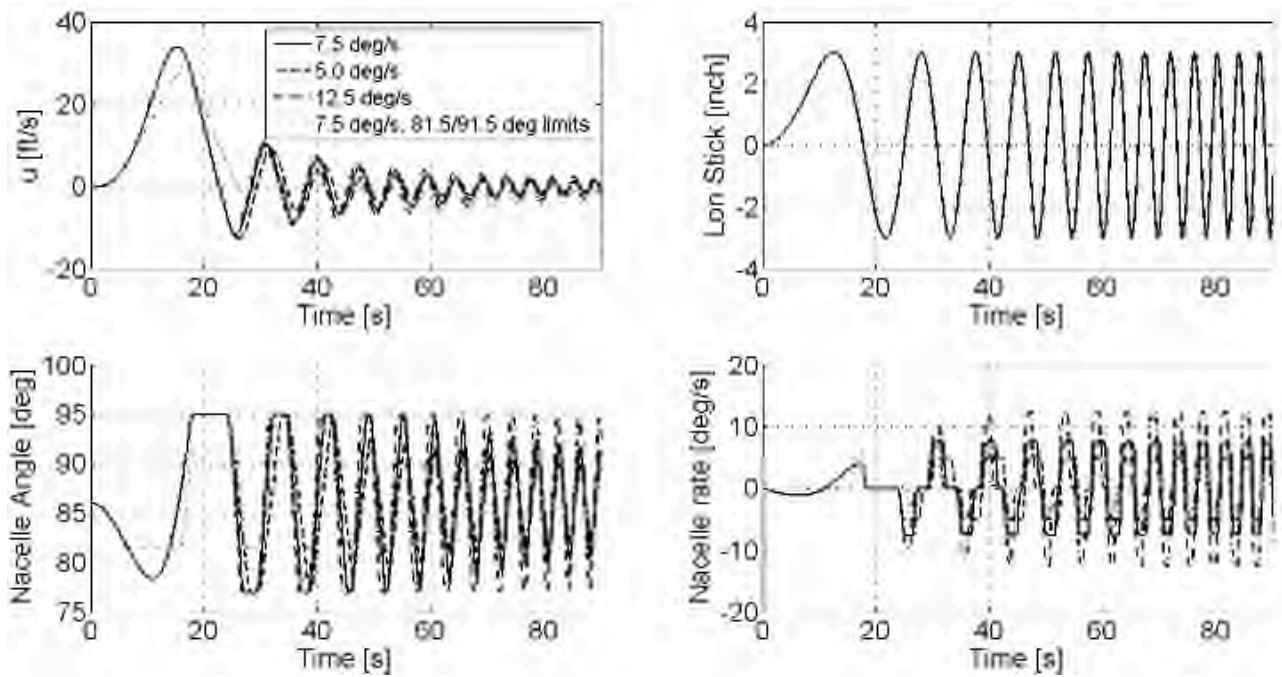
Figure 8: (a) Frequency response and (b) Time Response of longitudinal stick to body axis forward velocity, baseline TRC, varying input amplitudes

(a)

(b)

Figure 9: (a) Frequency response and (b) Time Response of longitudinal stick to body axis forward velocity u, 3 inch input amplitude, baseline TRC, varying nacelle actuation limits

As the nacelle actuator rate limits are reduced, as shown in Figure 9 (a), a similar trend to the increasing input amplitude is observed. For example, for the 5 deg/s limit configuration, a similar phase droop that crosses the 135 degree phase angle occurs, and thus confers a greatly reduced phase margin (~0.56 rad/s). The 7.5 deg/s rate limited control law has also a reduced bandwidth at the 3 inch input amplitude used, as already shown in Figure 8(a), but the rate limit of 12.5 deg/s, and the reduced position limit configuration (81.5 forward to 91.5 deg aft angle limits) maintain their phase bandwidths at approximately the same level as the 7.5 deg/s configuration at input amplitudes beyond 2 inches. This 'better' performance of the increased nacelle rate limit configuration is expected as it allows the nacelle angle to continue to track the input up to higher frequencies and provide the acceleration to track the velocity command. How the reduced position limit control law maintains the bandwidth is less intuitive: At low frequencies, the output velocity does not track the input at all well, the cause for this is that nacelle angle reaches the position limit almost immediately (within the first input cycle) leading to a highly non-linear response – as indicated by the low coherence. However, at higher frequencies, the position limiting appears to help the response, as it reduces the lag in the velocity response that

occurs when reversing the input. It is the nacelle angle (not rate) that primarily generates the rate of change of velocity at frequencies below 10 rad/s and the position limit stops the nacelle angle from getting too far from the trim datum.

The lowest nacelle rate limit of 5 deg/s had the lowest bandwidth, and OLOP performance, and was theoretically expected to confer the lowest handling qualities ratings. However, the piloted simulations showed that other factors served to also reduce the handling qualities of configurations with higher nacelle rate limits. Examining Figure 6 again shows that although the 5 deg/s configuration has a computed 40% probability of being awarded a HQR5 or worse. Similar probabilities of HQR5 or worse are also computed for the 12.5 deg/s nacelle rate limit. This seems somewhat counterintuitive, as Figure 9 showed that this configuration had better bandwidth characteristics. However, the higher nacelle rate limit led to a large amount of coupled, un-commanded, pitching oscillations [6]. Figure 10 compares the 12.5 deg/s to the 7.5 deg/s nacelle rate limit configuration (both using baseline control law) in a Precision Hover MTE. It shows the pitch rate/attitude oscillations during the final hover point capture phase of the maneuver are greatly increased for the 12.5 deg/s configuration.
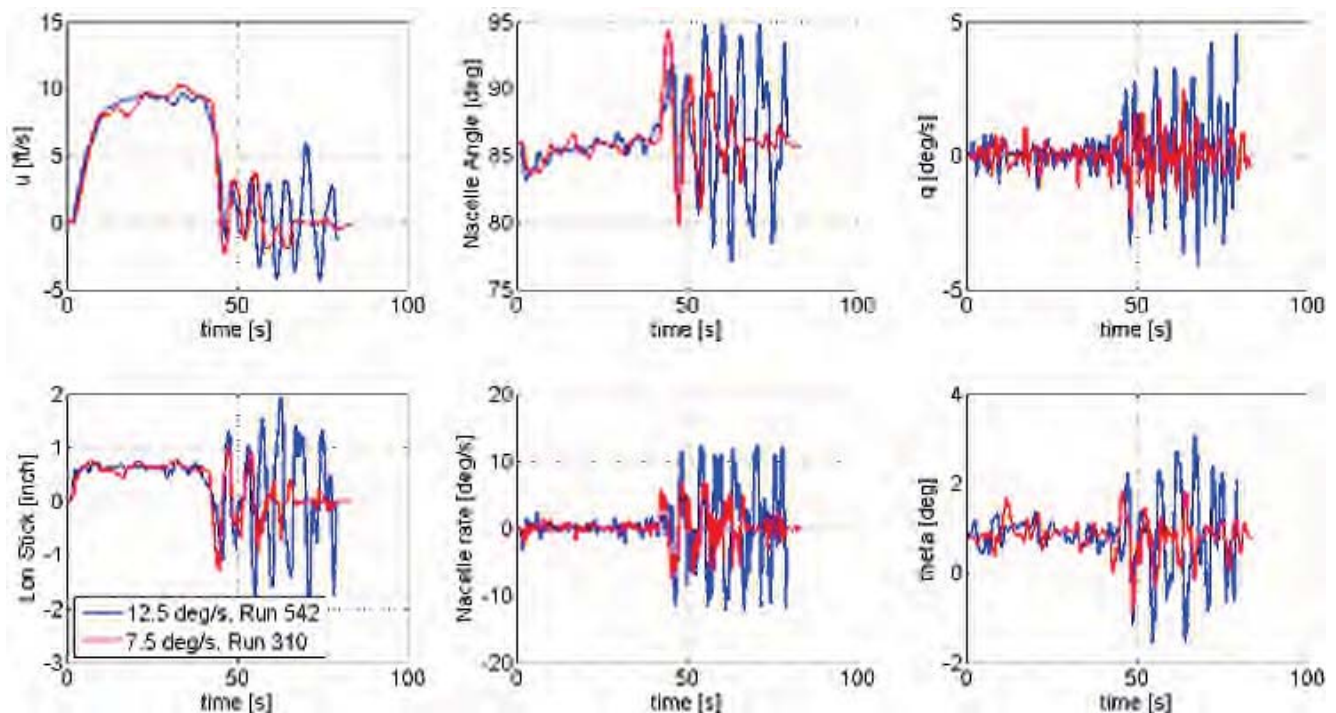

Figure 10: Comparison of time histories from VMS trials, baseline TRC, 12.5 deg/s vs. 7.5 deg/s nacelle rate limit

Nacelle Motion Coupling Effects

The oscillations were induced by the angular rate of the nacelles causing rotor flapping which in turn generated pitching moments on the aircraft body. To compound matters, the pitching motions are opposite in sense to the pilot input i.e. stick forward commands a forward rotation of the nacelles to accelerate forward, the rotors flap aft in response and cause a nose-up pitch (Figure 11). The larger the allowable nacelle rate, the larger the pitch disturbances.
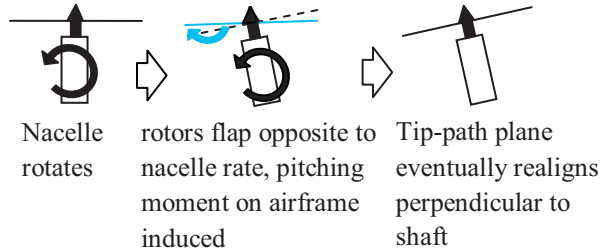

| Nacelle rotates | rotors flap opposite to nacelle rate, pitching moment on airframe induced | Tip-path plane eventually realigns perpendicular to shaft |

Figure 11: Illustration of sequence of flapping and pitching induced by nacelle rate

For some of the baseline TRC configurations the nacelle/flap/pitch coupling effect appeared only to be a minor 'nuisance' factor, especially as several pilots did not comment or notice it at all. Some pilots did comment on the perceivable aforementioned 'opposite sense' pitching that would occur with any longitudinal stick input. However, the scenarios where it became more obvious were where a PIO occurred, with a large amount of fore-aft motions, large stick inputs, and the nacelle actuators reaching their limits. The interconnected factors of nacelle rate limit and coupled pitching led to conflicting trends for the HQRs for the various TRC rate limit configurations – both increasing and decreasing the rate-limit could cause a reduction in HQR.

Nonetheless, it appeared that handling qualities improvements could be achieved by simply reducing the tendency to pitch with longitudinal stick inputs in TRC mode. The benefits foreseen through achieving a 'purer' response, i.e. translational motion only, included a better ride quality (as even small pitch motions were accentuated by the large pilot to c.g. offset), as well as 'clearer' motion cueing for the pilot.

Improved Translational Rate Command

To achieve this, a nacelle angular rate to rotor longitudinal cyclic 'crossfeed' was implemented (this is the improved model) – using a proportional gain that was 'tuned' to minimize the pitch response to longitudinal stick inputs in TRC mode. The improvement for the 12.5 deg/s configuration that suffered large pitching disturbances is clearly illustrated in Figure 12, showing a marked reduction in the peak pitch rate and attitudes. There was also notable reduction in stick input and subsequent nacelle motion activity, with fewer, smaller, oscillations, despite the maneuvers being flown with a similar aggression level (adjudged by the magnitude of the initial stick input and velocity profile of the deceleration phase). The control law models with the crossfeed feature improved the HQRs for all the configurations (Figure 6), even for those that did not suffer from excessive nacelle-pitch coupling that the crossfeed was designed to counter.
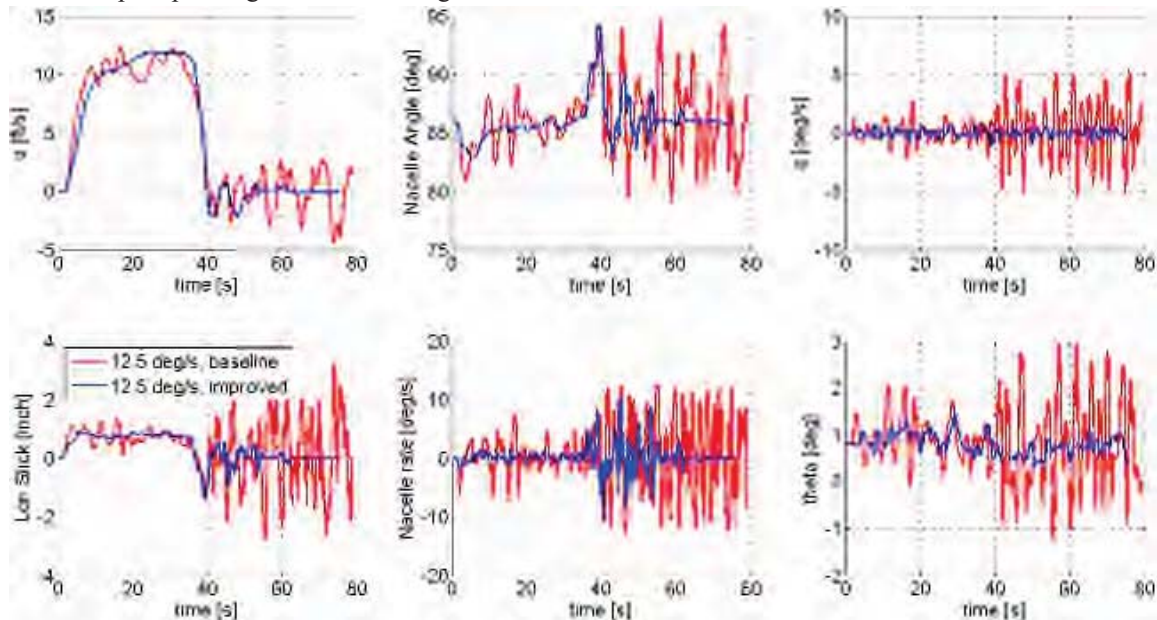

Figure 12: Comparison of time histories from VMS trials, 12.5 deg/s, baseline vs. improved control law
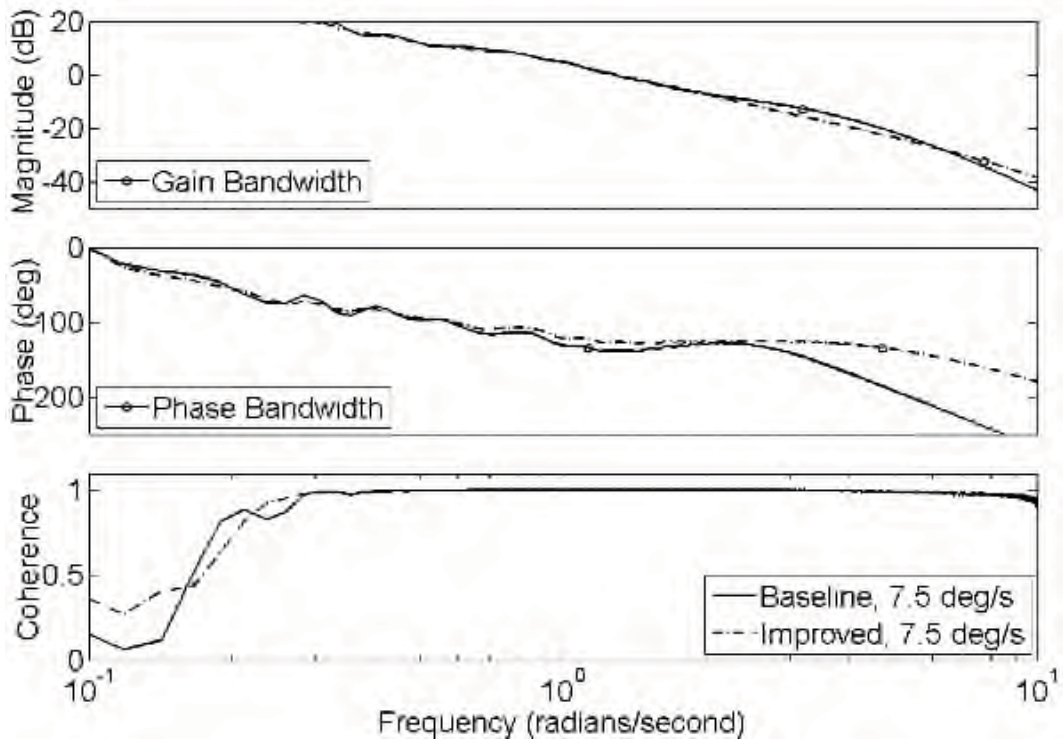
Figure 13: Frequency response comparison of longitudinal stick to body axis forward velocity u, 3 inch input amplitude, baseline and improved TRC control laws, 7.5 deg/s nacelle rate limit
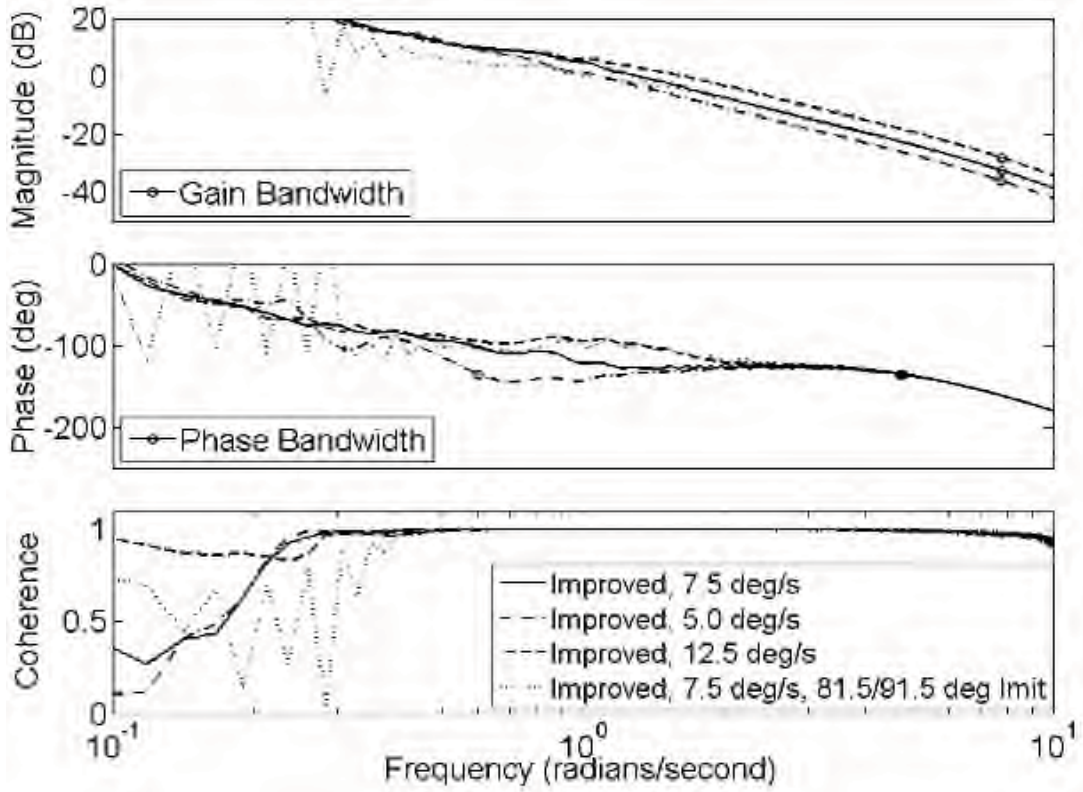

Figure 14: Frequency response comparison of longitudinal stick to body axis forward velocity u, 3 inch input amplitude, improved TRC control law with varying nacelle rate and position limits

The frequency responses in Figure 13 and Figure 14 help explain why nearly all the improved TRC configurations achieved superior HQRs. Figure 13 compares the baseline and the improved TRC control law at the 7.5 deg/s rate limit. It shows that the addition of the crossfeed causes an increase in the phase bandwidth by about 3 rad/s from just above 1 rad/s to around 4 rad/s. This is a significant improvement, which importantly, is maintained even at the higher amplitude 3 inch inputs. The increased bandwidth was found to produce a quicker or crisper response. This conferred insensitivity to pilot input aggression level, and a greater margin against instability under tight (high gain) control, including a reduced tendency to PIO.

Figure 14 compares the improved TRC at different rate limits. It shows that the phase bandwidths are essentially at the same ~4 rad/s level for all the configurations, except for the lowest nacelle rate limit. The complete trend in the bandwidths with varying input amplitude for the same configurations is shown in Figure 15. It confirms that the improved TRC has a higher bandwidth and maintains that bandwidth to higher stick amplitude levels at all the rate limits considered.

The correlation of input amplitude with the resulting handling qualities is further reinforced by the data presented in Figure 16. It shows two contour plots of the HQRs for the baseline and improved TRC configurations (with and without the crossfeed). The contours are a function of the pilot longitudinal stick cutoff

frequency and RMS amplitude. The pilot cutoff frequency gives a measure of the pilot operating frequency, and is defined as the frequency at the half power point of the total power spectral density of the pilot input [15]. This parameter has been shown to be a good estimate of the pilot crossover frequency in a closed loop flying task [16]. It is well known that the optimum piloted handling qualities are obtained when the pilot can function as a pure gain element in the closed-loop system [17]. This requires that the aircraft bandwidth exceed the piloted cutoff frequency. Otherwise, the pilot will be required to provide lead compensation and attendant increased workload. The frequency and amplitudes are calculated for the phase of the hover maneuver from which the pilot called 'stable' and thus represent the activity for the final position holding task of the Precision Hover MTE. The figure shows a classic spread of data points from low amplitude, high frequency inputs, moving through to the higher amplitude inputs only being achieved at lower frequencies. For the baseline control law without the crossfeed, the contours show that the regions of worse handling qualities ratings are strongly correlated with increasing amplitude and decreasing frequency. The comparison with the improved TRC control laws using the crossfeed is stark, with the range of stick amplitudes much reduced, reaching only around 1 inch. The range of cutoff frequencies are also reduced but to a lesser degree. The improvement in HQRs achieved is again very clear with a majority of the regions indicating Level 1 HQs.
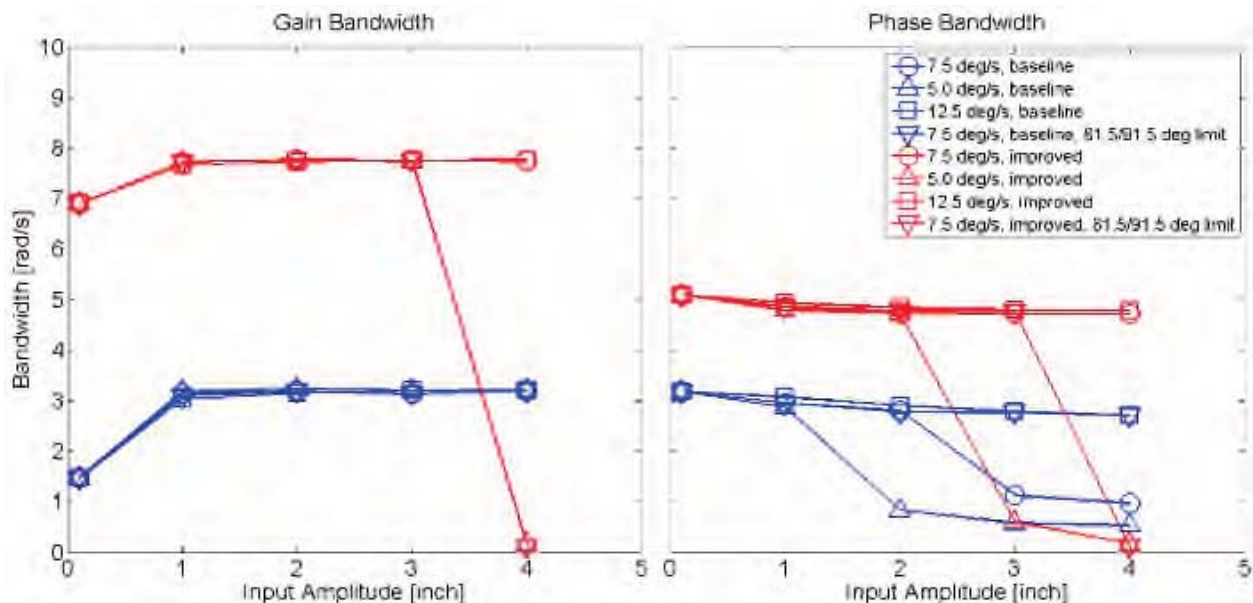

Figure 15: Gain and Phase Bandwidth for the LCTR2 TRC configurations at varying input amplitudes
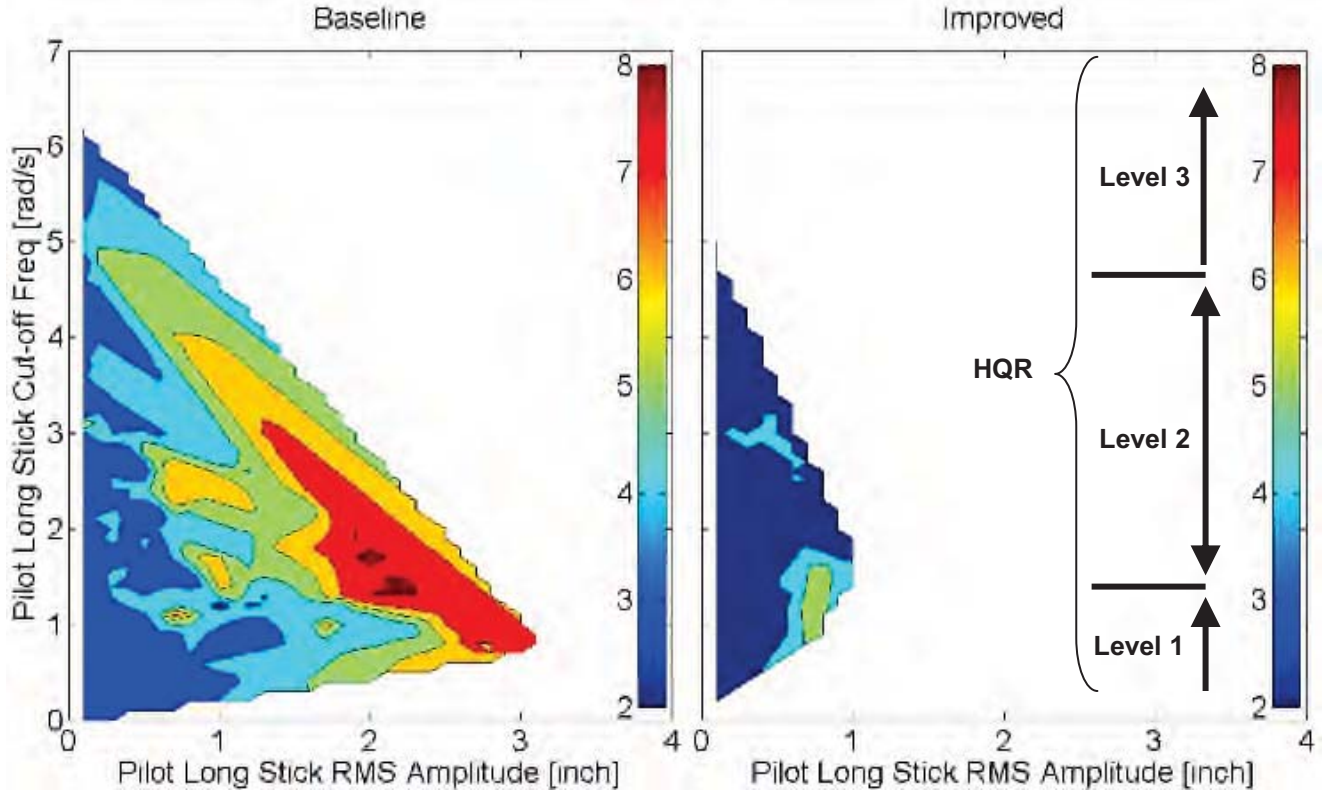
Figure 16: Contour plot of HQRs for varying pilot longitudinal stick input cut-off frequency and RMS amplitude for stabilised hover phase of Precision Hover MTE – compares baseline and improved TRC

Thus far, it has been shown that for the baseline TRC control law without the crossfeed, relatively subtle variations in nacelle actuator dynamics, and how aggressively the pilot flew, led to a large amount of variability in the handling qualities. It has also been shown that a relatively simple nacelle-rate-to-longitudinal cyclic crossfeed improved all the configurations, being insensitive to a variety of pilot techniques and aggression levels and virtually eliminated the PIO tendency that had previously existed.

Flight Dynamic Effect of Crossfeed

An analysis using a 1-degree-of-freedom linear perturbation model of the longitudinal motion in TRC provides useful insight into the flight dynamics aspects at work. There are a number of simplifying assumptions to the model, including that rotor flapping and airframe pitching is primarily only disturbed by nacelle inputs and that because of the primary attitude control loop, other pitch disturbances can be considered negligible when considering the longitudinal motion. As such, the equation of the motion, expressed in Laplace form is:

$$su = X_u u + X_{\beta_m}\beta_m + X_{\beta_{1c}}\beta_{1c} - g\theta \tag{1}$$

Here, the main influencing factors on the longitudinal body axis acceleration are the change in body axis forward speed, nacelle angle and rate (acceleration is neglected), rotor flap angle, and aircraft pitch attitude.

The equation of motion for the rotor flap is dependent on the nacelle angular rate, aircraft pitch rate, and the crossfeed gain, K, which inputs an amount of longitudinal cyclic proportional to the nacelle rate:

$$s\beta_{1c} = \dot{\beta}_{1c_{\dot{\beta}_m}} s\beta_m + \dot{\beta}_{1c_q} q + \dot{\beta}_{1c_{\theta_{1s}}}\theta_{1s} \tag{2}$$

$$\text{where } \theta_{1s} = Ks\beta_m$$

Therefore:

$$s\beta_{1c} = \dot{\beta}_{1c_{\dot{\beta}_m}} s\beta_m + \dot{\beta}_{1c_q} q + \dot{\beta}_{1c_{\theta_{1s}}} Ks\beta_m \tag{3}$$

Dividing by s and rearranging:

$$\beta_{1c} = (K\dot{\beta}_{1c_{\theta_{1s}}} + \dot{\beta}_{1c_{\dot{\beta}_m}})\beta_m + \dot{\beta}_{1c_q}\theta \tag{4}$$

$$\text{Where } q = s\theta$$

Substituting equation (4) into equation (1):

$$su = X_u u + X_{\beta_m}\beta_m + X_{\beta_{1c}}\left(K\dot{\beta}_{1c_{\theta_{1s}}} + \dot{\beta}_{1c_{\dot{\beta}_m}}\right)\beta_m + X_{\beta_{1c}}\dot{\beta}_{1c_q}\theta - g\theta \qquad (5)$$

The simplified pitch equation for hover assumes the dominant effect is rotor flapping:

$$sq = s^2\theta = M_{\beta_{1c}}\beta_{1c} \qquad (6)$$

Also substituting for β_{1c} here gives (4):

$$s^2\theta = M_{\beta_{1c}}(K\dot{\beta}_{1c_{\theta_{1s}}} + \dot{\beta}_{1c_{\dot{\beta}_m}})\beta_m + M_{\beta_{1c}}\dot{\beta}_{1c_q}\theta \qquad (7)$$

Solving (7) for the pitch attitude:

$$\theta = \frac{M_{\beta_{1c}}(K + \dot{\beta}_{1c_{\dot{\beta}_m}})\beta_m}{\left(s^2 - M_{\beta_{1c}}\dot{\beta}_{1c_q}\right)} \qquad (8)$$

Then substituting (8) into equation (5) gives:

$$su = X_u u + X_{\beta_m}\beta_m + X_{\beta_{1c}}\left(K\dot{\beta}_{1c_{\theta_{1s}}} + \dot{\beta}_{1c_{\dot{\beta}_m}}\right)\beta_m + \left(X_{\beta_{1c}}\dot{\beta}_{1c_q} - g\right)\frac{M_{\beta_{1c}}(K\dot{\beta}_{1c_{\theta_{1s}}} + \dot{\beta}_{1c_{\dot{\beta}_m}})\beta_m}{\left(s^2 - M_{\beta_{1c}}\dot{\beta}_{1c_q}\right)} \qquad (9)$$

Equation (9) shows the influence that the crossfeed gain, K has on the longitudinal dynamics. The convention is that the nacelle tilt angle, β_m, is negative for a forward rotation, so that the product of $X_{\beta_{1c}}\left(K\dot{\beta}_{1c_{\theta_{1s}}} + \dot{\beta}_{1c_{\dot{\beta}_m}}\right)\beta_m$ produces a negative X-acceleration when K is zero and the nacelles are rotated forward. This shows the retarding influence of $X_{\beta_{1c}}$ which is the longitudinal acceleration due to rotor flapping. This effect is linked directly to the flapping response to nacelle motion – when the rotors flap back against the nacelle tilt rate, the rotor thrust tilts accordingly. This means that the nacelle tilt responding to pilot commands has to work harder against the flap-back-induced thrust tilt. Selecting K such that $\left(K\dot{\beta}_{1c_{\theta_{1s}}} + \dot{\beta}_{1c_{\dot{\beta}_m}}\right) = 0$ eliminates this opposing acceleration effect.

The same effect is seen for the final term of equation (9) which represents the longitudinal acceleration due to pitch, in terms of the rotor flapping and nacelle dynamics derivatives. The mechanism is that the opposite sense pitching moment induced by the moving nacelles causes the aircraft to tilt in the X-Z-plane. In the body fixed frame, a gravitational component in the aircraft longitudinal axis manifests, whereas in the earth frame it is equivalent to the trim Z-axis force being tilted aft. In either frame of reference this action 'robs' the aircraft of some of the X-axis acceleration that it is trying to generate by tilting the nacelle – resulting in the nacelle having to rotate further/faster in order to achieve the commanded acceleration. Driving the term $\left(X_{\beta_{1c}}\dot{\beta}_{1c_q} - g\right)\frac{M_{\beta_{1c}}(K\dot{\beta}_{1c_{\theta_{1s}}} + \dot{\beta}_{1c_{\dot{\beta}_m}})\beta_m}{\left(s^2 - M_{\beta_{1c}}\dot{\beta}_{1c_q}\right)}$ to zero using the crossfeed gain eliminates this lagging effect.

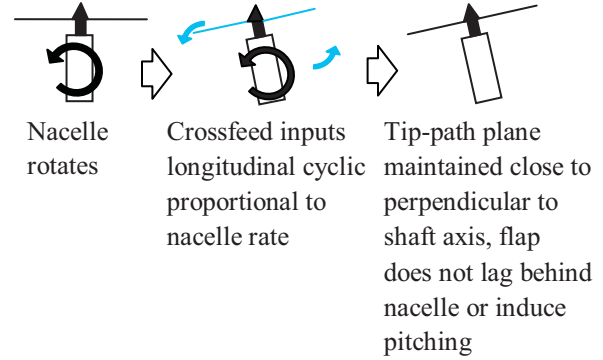| Nacelle rotates | Crossfeed inputs longitudinal cyclic proportional to nacelle rate | Tip-path plane maintained close to perpendicular to shaft axis, flap does not lag behind nacelle or induce pitching |

Figure 17: How crossfeed minimizes flapping and pitching induced by nacelle rate

The crossfeed is able to minimize the lagging effects on the longitudinal velocity of both rotor flap back to nacelle rate and the subsequent pitching motions by effectively keeping rotor disc plane perpendicular to the nacelle/shaft axis (Figure 17). Looking to future developments, additional longitudinal bandwidth or 'quickening' of the longitudinal velocity response might be achieved through increasing the crossfeed gain such that rotor disc tilt leads the nacelle tilt angle. However, such a scheme would reintroduce a certain amount of pitching motion, which although in the right directional sense, may bring back undesirable vertical accelerations for crew and passengers.

To summarize the analysis of the longitudinal TRC, it has been shown that the handling qualities were driven by a number of interdependent factors, including the nacelle rate and position limits, pilot input technique, and how aggressively the MTE was flown. This sensitivity to aggression also points to whether further consideration to whether the baseline ADS-33 MTE is appropriate to an aircraft of this size. It was also shown how the initial baseline control law was particularly sensitive to relatively subtle changes in these factors, and how the improved control law was able to make significant improvements to handling qualities.

TRC IN LATERAL REPOSITION

This section of the paper focuses on the lateral axis of the TRC control law in the Lateral Reposition MTE. Generally, this control law performed favorably. The control law consistently conferred level 1 handling qualities and was able to reduce the piloting task to almost a single control axis, 1-dimensional maneuver. As such, the lateral axis of the TRC can be treated almost independently of the longitudinal axis. Like for the Hover, the very large aircraft size warranted some modification to the baseline ADS-33E Cargo/Utility performance standards of the Lateral reposition MTE [7]. An increase in the time to complete the maneuver from 18sec to 25sec for *desired* performance [6] permitted the main objective, a reduction in the minimum groundspeed in the maneuver, 15kts instead of the usual 35kts. A wide variety of piloting techniques and aggression levels were applied without degradation of the HQRs.

In addition to the wings-level form of lateral TRC, a further control law was investigated in the Lateral Reposition that consisted of a 'Hybrid' mode that combined the lateral TRC with the lateral ACAH control law. This mode used a reduced gain of roll attitude per unit stick such that lateral stick commanded a small amount of roll angle in addition to the lateral velocity being regulated by lateral cyclic. The Hybrid mode was primarily developed in response to concerns that lateral speeds of up to 20kts would induce high levels of rotor flapping if driven by cyclic input alone. It was configured such that roll attitude changes were only commanded after the stick moved 1 inch, within this threshold, the aircraft behaved as under the baseline TRC.

A comparison of typical runs from the VMS piloted experiments using the different control laws is illustrated in Figure 18. The levels of roll angle, stick input and lateral flapping angles achieved are shown. The ease at which the maneuver was completed using TRC can be intimated from the lateral vs. longitudinal, and lateral vs. height position plots, where the aircraft maneuvers along almost 'perfect' straight lines. In comparison, the ACAH and the Hybrid modes both exhibit a certain amount of drift in longitudinal position and height. In terms of rotor flapping, the TRC and Hybrid modes both reach higher peak values (the solid and dotted lines are right and left rotors), reaching around ±6 degrees in the acceleration phase, and around ±10 degrees in the deceleration phase. In the intermediate phase where the lateral velocity is approximately constant, the flapping for ACAH is actually about the same magnitude as that for TRC, except with the direction on the rotors reversed (one being cyclic induced, the other flapping back to the oncoming flow). The Hybrid mode, as intended, shows smaller flapping angle than TRC for this phase of the maneuver, keeping close to the initial trim values. However, the peak values in the acceleration/deceleration phases are not significantly changed from those using TRC.
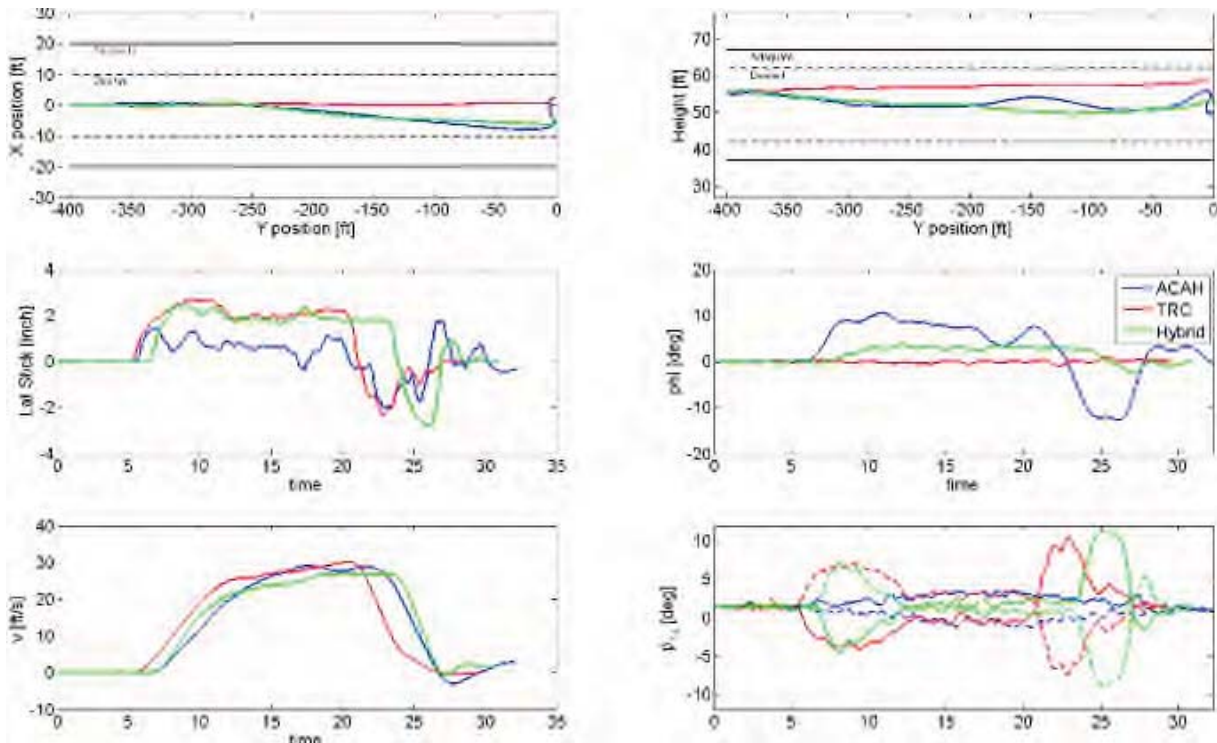

Figure 18: Piloted simulations comparing Lateral Reposition with ACAH, TRC and Hybrid control laws.

The model, based on linear stability derivatives, had a fairly simplistic representation of the lateral aerodynamics of the aircraft and was already showing reasonably large flapping angles to achieve the presented performance. Close to the hover point, the model's lateral dynamics were considered representative but as the sideward velocity increased it was recognized that there were likely to be deficiencies, especially an under-prediction of the airframe drag. The main impact of this would have been on the predicted levels of lateral cyclic input required as well the resulting lateral flapping angle. The flapping is of particular importance, because if this becomes excessive, then structural limitations or rotor to airframe collisions become of concern.

Simulations were conducted to assess the sensitivity to parameters that are important to representing the lateral aerodynamic drag characteristics. The stability derivative basis of the qLPV or 'stitched' model facilitated this analysis through the variation of terms such as Y_v to assess the impact of drag prediction on the lateral flapping in synthesized piloted Lateral Reposition maneuvers.

Pilot Modeling of Lateral Reposition

For this analysis the synthesized maneuvers were achieved through the use of a pilot model. The pilot model follows a similar architecture to that reported in Ref [18]. The key components are as illustrated in Figure 19. The model features two feedback loops, one outer and one inner loop that act on the observed longitudinal position and velocity respectively. The outer loop feedback signal is subtracted from a command signal that is a desired position trajectory. This error signal is passed through a pilot model outer-loop gain and lead/lag compensation to form the signal from which the inner loop feedback is subtracted. This error signal is then subject to an inner loop gain and a pilot time delay before input to the aircraft. Neuromuscular system dynamics and vestibular feedback cue model components were omitted for simplicity.

The advantage of using the pilot model is that it enables a repeatable set of parametric tests to be carried out but with an input profile that provides more insight than with simple open-loop inputs. Figure 20 shows the comparison of a number of runs using the pilot model where the Y_v derivative has been modified to a piloted run from the VMS experiments. It can be seen that the pilot model using the default Y_v replicates the shape and magnitude of the pilot inputs reasonably well and thus the aircraft under pilot model control tracks a similar velocity profile. This also results in the flapping response of the unadjusted model under pilot model and actual pilot control agreeing reasonably well. Doubling Y_v has a moderate effect on the flapping behavior as the peak flapping in the acceleration/deceleration parts of the maneuver is not really changed, the flapping is increased during the steady velocity part – the increment is not constant but a peak increase of around 2 degrees is seen. In the deceleration phase, there is a small decrement in flapping as the increased Y_v term now acts to help slow the aircraft and less cyclic input is required to decelerate. Quadrupling Y_v introduces a more significant effect. The flapping angles reached throughout the maneuver now approach the peak ±10 degrees only previously achieved in the deceleration phase.
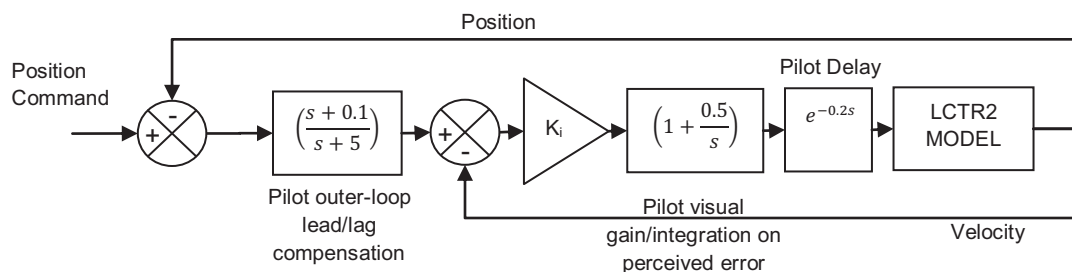

Figure 19: Block Diagram of pilot model used for Lateral Reposition analysis
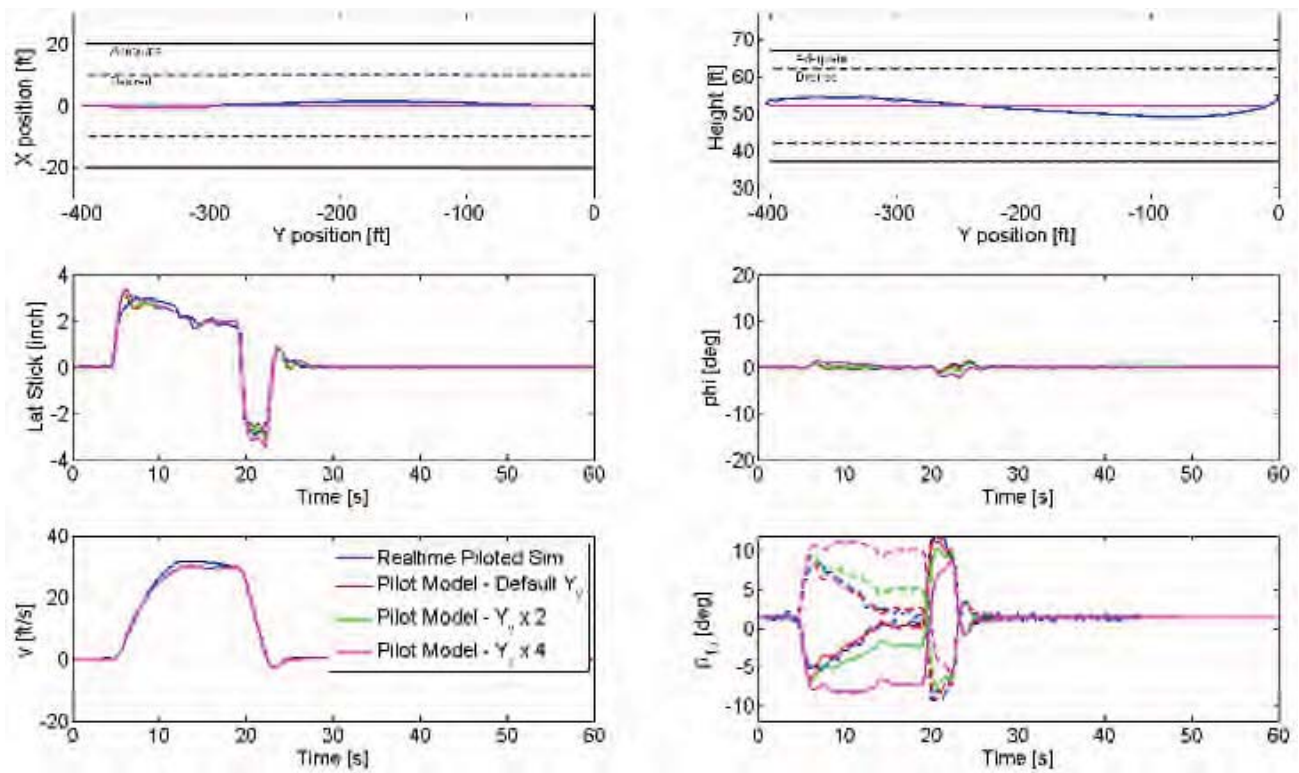
Figure 20: Comparison of time history of a piloted simulation from VMS experiments to simulated runs using a pilot model with varying Y_v characteristics in a Lateral Reposition MTE

A Y_v that is four times larger is estimated to be the amount required if the hover derivative is to represent the aerodynamic drag levels at 30 ft/s, which was approximately the peak lateral velocity achieved in most examples of the piloted experiments. Figure 21 illustrates this estimate by comparing the nonlinear drag computed for a reference area S=1 ft^2 and Drag coefficient C_D =1 with the equivalent linear stability derivative representation at the hover using a 7.7 ft/s perturbation size (the default value used for the stability derivative generation). It can be seen that the unmodified linear Y_v representation matches reasonably well with the nonlinear curve for small perturbations around the hover (up to around 10 ft/s) – reinforcing the validity of the approach for representing the hover. However, as the velocity increases the curves diverge from one another.

Linear Lateral Modeling Analysis

This result shows the limitations of the linear modeling approach for representing larger lateral velocities. However, improvements to the representation of the lateral aerodynamics within the existing model architecture can be made. The primary action would be to extend the qLPV model 'stitching' [5] to incorporate lateral velocity as another independent lookup variable. The model would then be able to represent the non-linear

changes in the trim states and controls with changing lateral airspeed and thus capture the effect of the nonlinear evolution of the steady trim forces and moments. Provided that the data for the lateral stitching (either from a high fidelity nonlinear model or flight-test data) is sufficiently accurate, the stitching process has been shown to be able to represent the nonlinear variation of the trim conditions [8].
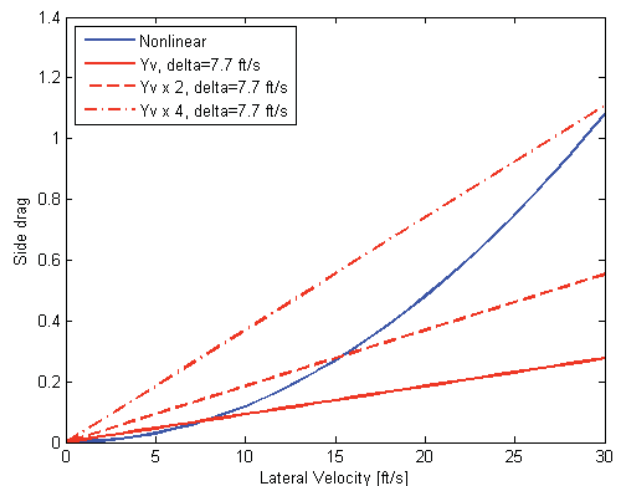

Figure 21: Comparison of non-linear to linear side force calculation

Command Model Effect on Flapping

Despite the likely under-prediction of drag it can also be shown that a significant amount of the peak flapping magnitude can also be attributed to how much acceleration is commanded by the control law. The following example helps explain the issue: In TRC mode, it can be assumed that the roll attitude is kept close to zero and that thrust variations with sideward velocity are a small percentage of the total (i.e. thrust is a constant). If the aerodynamic drag is ignored, a simple relationship between flap and acceleration demand can be defined where the side force is effectively proportional to the tilt of the rotor disc:

$$T\beta_{1s} = ma_y \qquad (10)$$

Rearranging:

$$\beta_{1s} = \frac{ma_y}{T} = \frac{a_y}{g} \quad \text{where} \quad T = mg \qquad (11)$$

From Figure 20, the pilot inputs can be approximated to 3 discrete phases: First, a step input of 2 inches to initiate the maneuver, which is then held steady until whereupon the stick is reversed for the deceleration and held at -2 inches (2nd phase) before finally being centered (3rd phase). For the 1st phase, the 2 inch input commands a target velocity of 30ft/s, the command model time constant for the first order TRC velocity response is 5 seconds [6]. Therefore an estimate of the lateral acceleration demanded, a_y is based on a linear acceleration to 63% of the commanded velocity in 5 seconds:

$$a_y = \frac{0.63 \times 2inch \times 15ft/s/inch}{5s} = 3.78ft/s^2 \qquad (12)$$

Using equation 11, the flapping required to generate the initial acceleration is approximately 6.7 degrees – which is a reasonably good estimate of the values observed in Figure 20. For the deceleration, the same calculation can be applied but the commanded velocity is based on a 4 inch stick input (from +2 inches to -2 inches) such that the flapping required to decelerate the aircraft is calculated to be 13.4 degrees. This value is a little larger than the delta in the flapping angle seen in the simulations which are around 10-11 degrees - the increased discrepancy can be attributed to the greater significance in the aerodynamic drag at the deceleration point.

In conclusion, accelerating and decelerating a ~100,000lb aircraft using lateral cyclic alone with time constants as recommended by ADS-33E [7] demands large lateral cyclic inputs and thus is a key driving factor behind the peak flapping levels in this maneuver. The analysis has shown that aerodynamic drag is likely to become a significant factor beyond around 15 ft/s, however, more sophisticated models are required to satisfactorily address questions about the aerodynamic drag influence on lateral flapping.

SUMMARY AND DISCUSSION

This paper has used both time and frequency domain analysis to illustrate the flight dynamic effects behind the handling qualities, including how a nacelle rate to rotor flap coupling effect influenced the longitudinal velocity response. Testing prior to the piloted experiments had identified the pitching response to longitudinal control inputs but it wasn't until the MTE-focused, piloted testing in a high fidelity motion-base system was carried out that the issues was really brought to the fore. The unusual control effector (automatic nacelle actuation) and airframe configuration (large pilot offset) meant that the typical 'rules of thumb' were not as reliable.

The Open-Loop Onset Point (OLOP) design criteria [14] predicted the likelihood of handling qualities deficiencies due to nacelle rate limiting. However, it could not have predicted the negative handling qualities outcome of increasing the nacelle rate limit with the original non-crossfeed configuration, as Figure 7 indicated the 12.5 deg/s configuration 'securely' in Level 1. These observations serve to reinforce the recognition of the engineering challenges that the LCTR2 configuration brings as well as highlighting the virtues of combined time and frequency domain analysis, and in particular of using piloted simulation with high quality motion-cueing.

The TRC architecture using automatic nacelle angle deflections with rate limits of ±7.5deg/s was shown to be a viable method (from a Handling qualities and flight control perspective) of providing longitudinal velocity control in hover and low speed whilst minimizing attitude changes.

The baseline TRC control law was able to provide handling qualities improvements compared to ACAH. However, a handling qualities 'cliff' featured where the aircraft was susceptible to PIO. Increasing pilot input amplitude increased nacelle rate and position limiting. This has been shown to cause a reduction in the bandwidth of the longitudinal velocity response to stick input and led to increased PIO tendency.

For the baseline TRC, rotor flapping induced by nacelle angular rate produced pitching moments opposite to the pilot stick inputs, i.e. stick (and nacelle) forward

would result in nose-up pitch. As nacelle rate limits were increased the pitching motions correspondingly increased.

The improved TRC (with nacelle rate to longitudinal cyclic crossfeed) not only reduced the pitching response to almost zero, but significantly improved longitudinal velocity bandwidth characteristics by minimizing the lagging effects caused by both the rotor flap back to nacelle rate and the subsequent pitching motions by keeping the rotor tip-path-plane plane perpendicular to the shaft axis. The improved TRC almost consistently achieved Level 1 handling qualities, and conferred a reduced sensitivity to pilot aggression levels and technique, virtually eliminating the PIO tendency, even for cases with reduced nacelle actuator rate limits.

In the Lateral Reposition MTE, the TRC control law induced lateral flapping angles generally within peaks of approximately ±10 degrees. The Hybrid mode led to a reduction of the flapping angle in the constant speed phase of the MTE but with little change in the peak flapping values in the acceleration and deceleration phases of the maneuver. The peak flapping levels were strongly influenced by the accelerations commanded by the control law command model. The peak flapping angle is also influenced by aerodynamic drag, however, it is more difficult to predict with the model currently available. To minimize increasing flapping due to large cyclic inputs, future investigation should continue with forms of Hybrid modes that mix roll attitude with lateral cyclic inputs.

CONCLUSIONS

- TRC using automatic nacelle angle was shown to be a viable method of providing longitudinal velocity control.
- The baseline TRC control law provided handling qualities improvements compared to ACAH.
- An improved TRC with nacelle rate to longitudinal cyclic crossfeed) reduced the pitching response to almost zero and significantly improved longitudinal velocity bandwidth characteristics.
- In the Lateral Reposition MTE, The peak flapping levels were strongly influenced by the accelerations commanded by the control law's command model response time constants.
- It is likely that the linear model used under-predicted the lateral drag and therefore the effect on predicted lateral rotor flapping for lateral translational flight above 15 ft/s (~10kts).

ACKNOWLEDGEMENTS

REFERENCES

[1] Johnson, W., Yamauchi, G.K, Watts, M.E, "NASA Heavy Lift Rotorcraft Systems Investigation", NASA/TP-2005-213467, NASA Ames Research Center, December 2005.

[2] Acree, Jr., C. W., Yeo, H., and Sinsay, J., Performance Optimization of the NASA Large Tiltrotor, NASA/TM-2008-215359, June 2008.

[3] Malpica, C.A., Decker, W.A., Theodore, C.R, Blanken, C.L., Berger, T., "An Investigation of Large Tilt-Rotor Short-term Attitude Response Handling Qualities Requirements in Hover", American Helicopter Society 66th Annual Forum, Phoenix, AZ, May 11-13, 2010.

[4] Blanken, C.L., Lusardi, J.A., Ivler, C. M. Tischler, M.B., Höfinger, M.T., Decker, W.A., Malpica, C.A., Berger, T., Tucker, G.E., "An Investigation of Rotorcraft Stability-Phase Margin Requirements in Hover", American Helicopter Society 65th Annual Forum, Grapevine, Texas, May 27 - 29, 2009.

[5] Lawrence, B., Malpica, C. A., Theodore, C. R., "The Development of A Large Civil Tiltrotor Simulation for Hover and Low-Speed Handling Qualities Investigations", 36th European Rotorcraft Forum, Paris, France, Sep 7-9th, 2010.

[6] Malpica, C. A., Decker, W.A, Theodore, C. R., Lawrence, B., Lindsey, J., Blanken, C.L. "An Investigation of Large Tilt-Rotor Hover and Low Speed Handling Qualities", American Helicopter Society 67th Annual Forum, Virginia Beach, VA, May 3 - 5, 2011.

[7] Anon., "Handling Qualities Requirements for Military Rotorcraft", Aeronautical Design Standard-33 (ADS-33E-PRF), US Army Aviation and Missile Command, March 21, 2000.

[8] Zivan, L., Tischler, M.B., "Development of a Full Flight Envelope Helicopter Simulation Using System Identification", Journal of the American Helicopter Society, Vol 55, No. 2, April 2010.

[9] Lusardi, J. A., Blanken, C. L., and Tischler, M. B., "Piloted Evaluation of a UH-60 Mixer Equivalent Turbulence Simulation Model," American Helicopter Society 59th Annual Forum, Phoenix, AZ, May 6-8, 2003.

[10] Bradley, R. and Maclaren, W. M., "A Better Way To Analyse And Interpret Helicopter Handling Qualities And Workload Ratings." 32nd European Rotorcraft Forum, Maastricht, Netherlands, 2006.

[11] Cooper, G. E. and Harper, R. P., "The Use of Pilot Rating in the Evaluation of Aircraft Handling Qualities," NASA TN D-5153, April, 1969.

[12] Liu, J. Q., Gao, Z.H., "A Test Evaluation of a Pilot-induced-Oscillation Prediction Criterion", 2nd International Conference on Signal Processing Systems (ICSPS), Dalian, China, 5-7 Oct, 2010.

[13] Aviation Safety and Pilot Control – Understanding and Preventing Unfavorable Pilot-Vehicle Interactions, National Research Council, National Academy of Press, Washington, D.C. 1997.

[14] Duda, H., "Prediction of Pilot-in-the-Loop Oscillations due to Rate Saturation", Journal of Guidance, Navigation, and Control, Vol. 20, No. 3, May-June 1997.

[15] Tischler, M. B., Remple, R. K., "Aircraft and Rotorcraft System Identification: Engineering Methods with Flight Test Examples," American Institute of Aeronautics and Astronautics, Reston, VA, 2006, pp-182-183.

[16] Anderson, F., Klyde, D.H., "A Limited Evaluation of the Pilot Cutoff Frequency Parameter", STI Working Paper No. 1310-13, Systems Technology, Inc., Hawthorne, CA, Sep 1997.

[17] McRuer, D. T. and E. S. Krendel, "Mathematical Models of Human Pilot Behavior", AGARD AG 188, STI-P-146, Systems Technology, Inc., Hawthorne, CA, Jan, 1974.

[18] Hess, R.A., Zeyada, Y., Heffley, R. K., "Modeling and Simulation for Helicopter Task Analysis", Journal of the American Helicopter Society, Vol., 47, No. 2, Oct., 2002, pp. 243-252.